Green Chemistry

Accepted Manuscript

ROYAL SOCIETY OF CHEMISTRY

www.rsc.org/greenchem

Oxidative desulfurization of DBT with H_2O_2 catalysed by TiO_2/porous glass

C. Shen[†], Y. J. Wang*[,‡], J. H. Xu[‡], and G. S. Luo*[,‡]

[†]Beijing Key Laboratory of Bioprocess, College of Life Science and Technology, Beijing University of Chemical Technology, Beijing 100029, China

[‡]The State Key Laboratory of Chemical Engineering, Department of Chemical Engineering, Tsinghua University, Beijing 100084, China

Corresponding author: Tel: 86-010-62788568, Fax: 86-010-62788568

Email address: wangyujun@tsinghua.edu.cn and gsluo@tsinghua.edu.cn

Abstract

Aimed at ultra-deep oxidative desulfurization (ODS) of dibenzothiophene (DBT) and 4,6-dimethyldibenzothiophene (4,6-DMDBT) to control air pollution, we specially designed and prepared porous glass supported with TiO_2 nanoparticles acting as an amphiphilic catalyst. Hydrogen peroxide which is considered as the "green" oxidant was used, and for the extreme liquid−liquid phase ratio (usually larger than 1500) reaction system, the pore volume of 0.19 mL/g of the catalyst provides enough space for storage of hydrogen peroxide. The as-prepared catalyst offers a high interfacial surface area of 116.9 m^2/g and enhances the reaction by facilitating the mass transfer. The mono-dispersed TiO_2 exhibited good crystallinity. The mean diameter varied from 2.1 to 7.8 nm with the loading amount increased from 1.27 wt.% to 9.85 wt.%. The catalyst showed high activity and good stability for producing ultra-clean fuels: 100% conversion was obtained within 2 min and the conversion just decreased from 100.0±1.0 % to 94.3±0.6 % after 5 cycles. Overall, this new reusable catalyst provided an alternative for highly efficient ultra-deep desulfurization in a green way.

Key words:

Ultra-deep desulfurization, Green oxidation, Supported TiO_2 nanoparticles, Catalytic performance

1. Introduction

Deep desulfurization of fuels has attracted more and more attention due to the increasing stringent regulations and specifications (<10 ppm). At the same time, fuel cell applications have also set forth stricter requirements of ultra-deep desulfurization (<1 ppm) [1,2].

As the major method in petroleum refineries to reduce sulfur content in fuels, hydrodesulfurization (HDS) is highly efficient in removing thiols and sulfides, but it meets critical challenges including: first, some refractory sulfur compounds, such as DBT and its derivatives are difficult to remove due to steric hindrance [3-6]; second, trace amount of sulfur compounds make deep-desulfurization extremely tough at the expense of significant decrease in octane number and increase in hydrogen consumption.

Therefore, there is an ongoing effort to develop alternative technologies. Various methods such as oxidation/photo-oxidation, adsorption, extraction, and distillation have been explored [7-26]. Among these, oxidation/photo-oxidation has attracted the most attention because of several attractive features, such as no hydrogen consumption, capability to remove the refractory sulfur compounds with relatively low cost of operation [7–22].

Hydrogen peroxide which is inexpensive and “green” is the best candidate as an oxidizing agent for liquid phase oxidation of sulfur compounds. However, ODS by hydrogen peroxide proceeds in two-phase system of immiscible liquids under extreme phase ratio of the organic phase to the aqueous phase (the phase ratio is usually larger than 1500): organosulfur compounds are present in the oil phase while hydrogen peroxide is located in the aqueous phase. As a consequence, the overall sulfur removal rate is limited by the mass transfer between phases with active catalysts. Phase transfer catalysts [10, 12, 27-36] have been considered as the potential way

to solve this problem. In these phase transfer reaction systems, the amphiphilic catalysts are assembled at the interface between the oil and aqueous phase where sulfur-containing compounds, hydrogen peroxide and catalysts interact with each other. The presence of the phase transfer agent notably facilitates the mass transfer at the polar-apolar interphase. But the phase transfer catalysts in the system are hardly separated from medium for reusing, and the stability of the catalysts should also be proved. These reasons inhibit further industry application of phase transfer catalysts.

TiO_2 has been widely used as the photocatalyst for ODS, due to the chemical stability, nontoxicity and inexpensiveness [19, 37-50]. After 10 hours of UV irradiation, 98.2% of DBT was removed using nano TiO_2 as the catalyst in Wang's work [19]. As reported by Zhu [51], the catalytic activity of amorphous TiO_2 powder was enhanced by adding hydrogen peroxide. 98% of organosulfur compounds were removed after 2 hours. However, the catalytic activity is still not high enough. This may be resulted from three aspects: first, it is well known that the particle size plays a significant role and the small size of TiO_2 is crucial to enhance the catalytic activity; second, aggregation of catalyst particles would also reduce catalytic activity. It is reported that TiO_2 powder agglomerates easily in reaction systems and the nano-sized TiO_2 particles should be deposited onto porous supports to maintain the catalytic activity [38-40]; third, the crystal phase is another key factor determining the catalytic activity. Many researchers have paid a lot of attention to antanse phased TiO_2 for their high adsorptive property for sulfur-containing compounds [52-60]. As reported by Guo et al. [52] and Watanabe et al. [53], both anatase (0 0 1) surface and (1 1 0) surface are confirmed to be adsorptive for sulfur compounds.

In this work, we specially designed porous glass beads supported with TiO_2 nanoparticles

which would act as an amphiphilic catalyst and explored the feasibility of using the as-prepared catalyst for ultra-deep desulfurization of DBT and 4,6-DMDBT under the extreme liquid-liquid phase ratio reaction condition. To the best of our knowledge, TiO_2 immobilized on porous glass beads has not been reported to be used as the catalyst for ODS yet. There may be three possible advantages by choosing porous glass as the support: first, because of the good ion-exchange property as proved in our previous work [61, 62], it is easier to make TiO_2 nanoparticles highly dispersed on the surface and pores of porous glass beads; second, as reported in our previous work [63], porous glass beads showed good adsorptive property for organosulfur compounds through polar interactions. So it would enhance the oxidation by better adsorption for the reactant, besides, the product namely sulfones with stronger polarity would also be adsorbed simplifying the ODS process easier. Similar result (sulfones can be removed with high capacity using common hydrophilic adsorbents) has also been reported by Timko and coworkers [22]; third, H_2O_2 aqueous solution would be fixed in the pores of porous glass beads. The large pore volume could be used for storage of water soluble reactants. Hence, based on the adsorptive property for both the two reactants, porous glass supported with TiO_2 would act like an amphiphilic catalyst as shown in Figure 1. The as-prepared catalyst provides high interfacial surface areas where the chemical reaction takes place and improves the reaction performance. Besides, easy separation becomes available at the same time by filtration. The solution of DBT or 4,6-DMDBT dissolved in octane was used as the model fuel. Effects of reaction duration, catalyst content, initial concentration, oxidant amount, and reaction temperature have been studied systematically in relation to the conversion. And the regeneration performance of the catalyst has been investigated as well.

2. Experimental

2.1. Materials and chemicals

Soda-lime glass microbeads with diameters ranging from 75 μm to 150 μm and composed of 59.7 wt.% SiO_2, 25.1 wt.% Na_2O, 9.8 wt.% MgO, and 4.9 wt.% CaO were obtained from Hebei Chiye Corporation. The beads were sieved before application, and beads with sizes ranging from 95 μm to 105 μm were taken as samples. Titanium oxysulfate was purchased from Beijing Chemical Plant. Analytical grade octane was purchased from Fuchen Chemical Plant in Tianjin, China. DBT was purchased from Acros Organics. All chemicals were used as received without further treatment.

2.2. Preparation and characteristic of porous glass beads supported with TiO_2 nanoparticles

The porous glass beads were prepared by the subcritical water treatment method described in our previous study [61, 62]. First, 200 g of water and 5 g of glass beads were placed in a tank reactor with a volume of 250 cm^3. The reactor was then gradually heated to 573±0.1 K, and the pressure was increased from atmospheric pressure to almost 8 MPa. The subcritical state was maintained for 60 min, and then the reactor was cooled naturally to room temperature. Afterward, the porous glass beads were washed several times with deionized water.

Different amount of titanium oxysulfate (ranged from 0.1 to 2.0 g) was dissolved in 70 g of deionized water. Then 1.5 g of the porous glass was added into the solution. The mixture was shaken for 24 h at 160 rpm in a temperature-controlled shaker at 303 K. The porous glass beads were separated from the solution by filtration and then washed with deionized water several times. After the porous glass beads were dried, they were calcinated from 303 K to 773 K with a heating speed of 1 K/min and remained at 773 K for 2 hours.

The morphology of the porous glass beads supported with TiO_2 nanoparticles was observed via SEM (HITACHI S-4500, HITACHI Ltd., Japan). TEM images were generated with a JEOL JEM-2011 high-resolution transmission electron microscope. The diffused reflectance spectra of the samples over a range of 200 nm to 800 nm were recorded by a HITACHI U-3900 spectrophotometer with $BaSO_4$ for reference. The Ti element in the whole composite material was detected through ICP (ICP, IRIS Intrepid II XSP from ThermoFisher Corp., USA). Nitrogen adsorption-desorption isotherms were measured at 77 K on a Quantachrome Autosorb-1-C Chemisorption-Physisorption Analyzer. The specific surface area was calculated from the adsorption branches in the relative pressure range of 0.05 to 0.25. The pore diameter and pore size distribution were calculated from the desorption branches using the Barrett-Joyner-Halenda (BJH) method. The total pore volume was evaluated at a relative pressure of approximately 0.99. The catalyst was also characterized by X-ray photoelectron spectroscopy (XPS).

2.3. Oxidative desulfurization

DBT oxidation was performed in a 150 mL glass-stirred reactor equipped with a water-circulated condenser column. The reactor was immersed in a water bath to keep the reaction temperature constant. A magnetic stirrer was used to blend the reaction mixture. In order to exclude the effect of mass transfer (both external diffusion and internal diffusion), two groups of experiments were carried out to determine the stirring speed and size of porous glass. In the first group of experiment, porous glass beads with the mean size of 100 μm were used as the support. Effect of stirring speed on conversion of DBT was investigated. And in the second group of experiment, effect of support size was explored. The results are shown as Figure S1(a) and S1(b), respectively. Results indicated that when the stirring speed was larger than 550 rpm, the effect of

external diffusion could be neglected, and when the support was smaller than 200 μm, the effect of internal diffusion could be neglected. Therefore, the stirring speed and the support size were chosen as 750 rpm and 100 μm, respectively during the whole reaction process. In a typical run, 1.0 g of the prepared catalyst and 35 g of the model fuel with DBT concentration of 150 ppm were added in the reactor and heated for 5 min. 29 μL of hydrogen peroxide with the concentration of 30 wt.% (the molar ratio of H_2O_2-to-DBT was 10, the volume ratio of the organic phase to the aqueous phase was 1724) was then added into the reactor to start the reaction. Samples were taken after different reaction durations.

The reaction product was analyzed by gas chromatography (GC) 2014 with an FPD detector (SHIMADZU). The chromatographic column is Rat-Wax. The injector and the detector temperatures were both set to be 553 K. The oven temperature was maintained at 503 K for 5.3 min. Nitrogen gas with a flow rate of 30 mL/min was used as the carrier gas. The flow rate of hydrogen gas and air were 30 and 300 mL/min, respectively. DBT conversion and space-time yield are defined as Equations (1) and (2), respectively.

$$X = \frac{\Delta n_{DBT}}{n_{0DBT}} \qquad (1)$$

$$STY = \frac{g_{DBTS}}{g_{TiO_2} \times t} \qquad (2)$$

where Δn_{DBT} is the amount of DBT converted with the mole unit, n_{0DBT} is the amount of DBT introduced with the mole unit. g_{DBTS} and g_{TiO_2} are the mass amounts of DBTS and TiO_2, respectively, and t is the reaction duration.

3. Results and discussion

3.1. Characteristics of porous glass beads supported with TiO_2 nanoparticles

Surface morphologies of glass beads before and after the subcritical water treatment is shown as Figure S2 and Figure S3, respectively. BET results are listed in Table S1 in the supporting material. Glass beads were smooth and compact before the subcritical water treatment and the surface area was just 2.9×10^{-3} m^2/g. While after the subcritical water treatment, the outer layer of glass beads become porous, besides both the surface area and pore volume are greatly increased. Surface morphologies of the porous glass beads supported with TiO_2 nanoparticles are shown in Figures 2(a) and 2(b), respectively. After TiO_2 immobilization, the porous glass beads retained their spherical shape.

The pore size distribution of glass beads supported with TiO_2 nanoparticles is shown in Figure 2(c). The specific surface area of the catalyst reached 116.9 m^2/g. The pore volume and the mean pore diameter are 0.19 mL/g and 6.50 nm, respectively.

The XRD pattern of porous glass supported with TiO_2 nanoparticles shown in Figure 3 matched well with the standard card of the anatase phase (JCPDS No. 78-2486). Typical diffraction peaks detected at 25.3 º, 37.8 º, 48.0 º, 55.1 º, 62.7 º, and 75.1 ºare attributed to (101), (004), (200), (211), (204), and (215) planes of anatase TiO_2 crystals, respectively indicating that the prepared TiO_2 nanoparticles in the present study have the anatase phase.

The coordination state of Ti species was investigated by UV-vis spectroscopy as shown in Figure S4 in the supporting material. Peaks around 240 nm to 330 nm are attributed to small TiO_2 clusters through the quantum size effect [64,65].

The binding energy of Ti element was measured by XPS to take a deeper insight into the state of incorporation of Ti species in the framework. As shown in Figure S5 in the supporting material,

Ti $2p_{3/2}$ peak at 458.6 eV is due to the presence of octahedral coordination of Ti ions [66]. Combining with results of XRD and UV-vis, it is confirmed that TiO_2 nanoparticles are supported on the porous glass.

Porous glass beads with different Ti contents have been prepared by varying the mass of titanium oxysulfate. The amount of Ti in the whole composite ranged from 1.27 wt.% to 9.85 wt.% determined by ICP.

TEM images of supported TiO_2 nanoparticles are shown in Figure 4. The TEM images shows a perfectly crystalline nanocrystal and lattice fringes with a width of 0.34 nm are clearly observed in Figures 4(a) which would be contributed to the (110) plane of anatase. TEM images of supported TiO_2 nanoparticles with the Ti content of 1.27 wt.%, 3.67 wt.% and 9.85 wt.% are shown as Figures 4(b), 4(c) and 4(d), respectively. And the corresponding histograms of particle size distributions are given in Figures 4(e), 4(f) and 4(g), respectively. The histograms were derived from the TEM images by surveying more than 150 particles. And imageTool v3.0 software was used to measure particle sizes in the TEM images. The average TiO_2 particle size was quantified based on a number-weighted diameter ($\bar{d} = \sum n_i d_i / \sum n_i$, n_i is the number of counted TiO_2 particles with a diameter of d_i) with values of 2.1 nm, 2.8 nm and 7.8 nm for catalysts with Ti contents of 1.27 wt.%, 3.67 wt.% and 9.85 wt.%, respectively. Obviously, TiO_2 nanoparticles prepared in this work exhibited small mean particle size and narrow size distribution which might be of great help for improving the catalytic activity.

3.2. Catalytic activity for removal of DBT

As shown in Figure 5, the porous glass beads supported with TiO_2 nanoparticles exhibited high catalytic activity. Compared with the reaction duration, the Ti content in catalyst shows much

profounder effect on conversions. When the Ti content increased from 1.27 wt.% to 6.45 wt.%, big jumps in conversions were observed. Only 33% of DBT was converted in 1 min with the Ti content of 1.27 wt.%, and the conversion was promoted to be 63% when the Ti content increased to 3.67 wt.%. For the catalyst with Ti content of 6.45 wt.%, 90% of DBT was converted just in 1 min, and complete conversion would be obtained within 2 min. As shown in Figures 4(b) and 4(c), when the Ti content increased from 1.27 wt.% to 3.67 wt.%, the change in mean particle size of TiO_2 is minor, while the amount of active centers is bigger. This may explain the enhanced reaction rate when the Ti content varied from 1.27 wt.% to 6.45 wt.%. However further increase in Ti content resulted to a reaction rate reduction. Catalysts with the highest Ti content of 9.85 wt.% showed even worse performance than the catalyst with Ti content of 8.24 wt.%. This may be due to three possible reasons: first, the largest crystal size of TiO_2 as shown in Figure 4(d); second, rapider decomposition of hydrogen peroxide using catalyst with higher Ti content. Comparisons in H_2O_2 decomposition rate using catalysts with different Ti content are shown as Figure S6 in the supporting material; third, the smallest surface area as listed in Table 1.

The contribution of adsorption by the catalyst was also investigated as shown in Figure 5. Catalyst with Ti content of 6.45 wt.% was used as the adsorbent, and a removal rate of only 3.9% was obtained after 8 min. Therefore, the high removal rate of DBT was mainly contributed to the chemical oxidation. As shown in Figure 1, TiO_2 nanoparticles supported on porous glass beads decompose H_2O_2 and form the appropriate Ti-peroxo intermediates which render the reactive oxygen species for the oxidation of the organosulfur compounds to the corresponding sulfones. Similar results have also been reported by Cedeno-Caero [67].

Comparisons in catalytic activity with P25 and silica supported with P25 with the as-prepared

catalyst are shown in Figure S7 in the supporting material. During the experiments, the amount of TiO_2 was kept to be 0.1 g. Other conditions were the same with experiments shown in Figure 5. Compared with porous glass beads supported with TiO_2 nanoparticles, both P25 and silica supported with P25 showed less catalytic activity. P25 immobilized on the surface of silica behaved better than those in the suspension mode. Maybe it is resulted from better dispersion of TiO_2 in the immobilization mode.

Removal of DBT has been conducted in other studies [19,37,38,40] using TiO_2 particles as the catalyst. Comparisons in catalytic performances in these studies are listed in Table 2. The space-time yield has been increased by one or two order of magnitude without UV irradiation.

The excellent catalytic performance of TiO_2 nanoparticles supported on porous glass beads was mainly contributed to three reasons. Besides the small particle size and the crystal phase (anatase) of TiO_2 nanoparticles, the support also played a significant role. Due to the adsorptive property for both the two reactants, it made enhancement in catalytic efficiency become available. Porous glass beads immobilized with TiO_2 nanoparticles provided high interfacial surface areas where the oxidation took place and improved the reaction by reducing the interphase mass transport. In order to improve the hypothesis, two groups of experiments were designed. In the first group, TiO_2 powder was prepared through hydrolysis of tetrabutyl titanate (TEOT). The preparation was described in detail in the supporting material. TEM image, the corresponding histogram of particle size distribution and XRD pattern of the TiO_2 powder are shown as Figure S8(a), S8(b) and S8(c), respectively. Obviously, TiO_2 nanoparticles prepared by the hydrolysis of TEOT show bigger mean particle size (10.9 nm) compared with those supported on porous glass beads through ion exchange process. According to our previous work [54], porous glass beads could be modified by

hydrochloric acid for the removal of alkali metal and alkaline-earth metals contained in the shell part. After the modification, the FT-IR spectra closely matched that of SiO_2 powder. Besides, the adsorptive capacity for organosulfur compounds of porous glass beads after the treatment with HCl was neglectable. And then the as-prepared TiO_2 powder was immobilized on porous glass beads and porous glass beads after the HCl treatment through suspension method, respectively. So TiO_2 particles in the suspension mode and the immobilized ones have the same particle size and crystal form. Their catalytic performances are shown in Figure 6 (a) and the amount of TiO_2 was kept the same during the experiments. As expected, TiO_2 in the immobilized modes showed higher activity compared with those in the suspension mode, notably, TiO_2 supported on porous glass beads without HCl treatment exhibited the highest catalytic activity. The result confirmed our hypothesis that using porous glass (with good adsorptive property for organosulfur compounds) as the support would enhance the catalytic activity; in the second group, the catalyst prepared by the ion exchange method (porous glass beads supported with TiO_2 nanoparticles) was hydrophobicated with hexamethyldisilazane. The contact angle changed from 0 °to 154 °after the surface modification. If our hypothesis were true, with the increase in contact angle, adsorption capacity for H_2O_2 aqueous solution would decrease resulting in decrease in catalytic activity. And their catalytic performances are shown in Figure 6 (b). With the increase in contact angle, apparent decrease in catalytic activity was observed. Especially the catalyst with the contact angle of 154 ° showed little catalytic activity. In a nutshell, the experimental results confirmed the hypothesis that based on the proper physical property of the heterogeneous catalysts, porous glass beads supported with TiO_2 would act like amphiphilic catalyst. Easy separation as well as enhancement of catalytic efficiency becomes available by using this novel catalyst. It provides highly promising

alternative for highly efficient ultra-deep desulfurization in a green way.

3.3. Effect of initial concentration on conversion

Catalytic performances of porous glass beads supported with TiO_2 nanoparticles under various initial sulfur concentrations are presented in Figure 7. With the increase of initial concentration, the conversion decreased. Complete conversion has been obtained within 50 s when the initial concentration was 50 ppm. But only 73% of DBT was converted at 50 s with an initial concentration of 100 ppm.

3.4. Effect of oxidant amount on conversion

The effect of the oxidant amount was determined in relation to the changes in DBT conversion, as shown in Figure 8 (a). With the increase in the mole ratio of H_2O_2-to-DBT, the reaction rate first increased and then decreased. When the ratio of H_2O_2-to-DBT was not bigger than 10, the reaction rate was greatly fastened through adding more H_2O_2, and it may be resulted from production of more Ti-peroxo intermediate. However, further increase in oxidant reduced the reaction rate. It is because that introduce of large amount of H_2O_2 aqueous solution against the adsorptive property for organosulfur compounds. With the increase in H_2O_2 amount, more and more surface areas were occupied by the aqueous solution, and it resulted in both the decrease in adsorption property for sulfur compounds and agglomeration of catalysts. Even if the TiO_2 nanoparticles have formed the Ti-peroxo intermediates, it was too hard for them to contact with sulfur-containing compounds. In other words, the utilization efficiency of the Ti-peroxo intermediates is far lower. Of course, to some extent this problem could be solved by increasing the mixing speed. TiO_2 nanoparticles could transport between the organic and water phases and catalyze the reaction slowly under vigorous stirring. That explains the low catalytic activity of

TiO_2 powders as reported by other works. Distributions of porous glass beads supported with TiO_2 in the model oil with different amount of H_2O_2 aqueous solution are shown in Figure 8(b) and 8(c), respectively. Porous glass beads supported with TiO_2 nanoparticles distributed homogeneously in the model oil when the H_2O_2 amount was 29 μL (Figure 8(b)), while agglomerated together and attached to the bottom when 0.19 mL of H_2O_2 was added (Figure 8(c)). The latter showed little catalytic activity (the removal rate was only 4.43% after 7 min).

3.5. Effect of reaction temperature on conversion

The effect of reaction temperature was investigated, and the results are shown in Figure 9(a). When the temperature increased from 303 K to 333 K, the reaction was obviously enhanced. The conversion of DBT increased from 32% to 60% when the reaction temperature varied from 303 K to 333 K, with fixed reaction duration of 100 s.

It is reported that ODS would be described by a pseudo-first kinetics order, which is rationalized in terms of the Langmuir-Hinshelwood model, modified to be valid for reactions occurring at a solid-liquid interface, [19,37-39, 68-70]. The reaction rate can be described by Equation (3).

$$r_0 = -\frac{dC}{dt} = \frac{k_r K C_{eq}}{1 + K C_{eq}} \quad (3)$$

where r_0 is the initial rate of disappearance of DBT and C_{eq} is the equilibrium bulk-solute concentration. K represents the equilibrium constant for adsorption of DBT onto TiO_2 surface and k_r reflects the rate constant of deposition of DBT. This equation could be used when data demonstrate linearity plotted as follows:

$$\frac{1}{r_0} = \frac{1}{k_r K} \times \frac{1}{C_{eq}} + \frac{1}{k_r} \quad (4)$$

The apparent pseudo-first-order values and Langmuir-Hinshelwood parameters obtained under different temperatures are listed in Table 3 and Table 4, respectively.

Based on the Arrhenius equation, the activation energy (E) can be calculated using Equation (5).

$$\ln k = \ln k_0 - \frac{E}{RT} \qquad (5)$$

where k_0 is the frequency factor or pre-exponential factor (s^{-1}).

The plot of lnk_r versus 1/T is shown in Figure 9(b) with the R^2 value of 0.9993. The activation energy was calculated from the slope with the value of 60.1 KJ/mol.

3.6. Oxidation of 4,6-DMDBT

The methylated derivatives of DBT are considered to be the most refractory compounds in HDS. In this work, oxidation of 4,6-DMDBT was investigated as well. Figure 10 illustrates that 4,6-DMDBT could also be effectively oxidized. The conversion increased along with the prolonging of reaction time, and complete conversion was obtained after 5 min.

3.7. Regeneration performance

Desulfurization catalysts must be regenerated for multiple cycles. Results of the regeneration test are shown in Figure 11. The used catalyst was calcinated for 2 h at 773 K. Compared with the fresh catalyst, the conversion decreased a little from 100.0 ±1.0 % to 94.3 ±0.6 % after five cycles. The ease of regeneration of the as-prepared catalyst indicates that it is suitable and feasible in practical applications.

4. Conclusion

In order to control air pollution caused by organosulfur compounds contained in fuels, porous

glass supported with TiO_2 nanoparticles was successfully prepared and it acted as a novel amphiphilic catalyst for ultra-deep ODS of DBT and 4,6-DMDBT in a green way. It has been proved by experiments that the support which showed good adsorptive property for both reactants helped to gather the two reactants on the active sites. The as-prepared catalyst provided high interfacial surface areas where the oxidation took place and promoted the reaction by enhancing the interphase mass transport. The supported TiO_2 nanoparticles prepared in this work exhibited good crystallinity. The mean crystal size varied from 2.1 to 7.8 nm with the loading amount increased from 1.27 wt.% to 9.85 wt.%. Effects of reaction duration, catalyst content, initial concentration of DBT, oxidant amount and reaction temperature on conversions were investigated systematically. The Ti content was optimized to be 6.45 wt.%, and complete conversion of DBT with an initial concentration of 150 ppm was obtained within 2 min. DBT oxidation by supported TiO_2 nanoparticles followed a pseudo-first-order kinetics according to the Langmuir-Hinshelwood model with the activation energy of 60.1 KJ/mol. The apparent rate constant was increased by one to two orders of magnitude compared with other studies. The catalyst also showed good regeneration performance with the conversion decreased from 100.0 ± 1.0 % to 94.3 ± 0.6 % after five cycles. TiO_2 nanoparticles supported on porous glass beads are pollutant-free-prepared, low-cost, and highly catalytic active, and are thus proving highly promising for producing ultra-clean fuels. To understand the catalytic mechanism deeply, further studies should be conducted such as the search for the transition state and responses of different sulfur containing compounds during the ODS process. Besides, how to increase the utilization of H_2O_2 is also worth of serious consideration.

Acknowledgements

We gratefully acknowledge the support of the National Basic Research Foundation of China (Grant No. 2013CB733600) and the National Natural Science Foundation of China (91334201, 21036002, 21276140).

References

[1] E. Ito, J. A. R. Van Veen, *Catal. Today*, 2006, **116**, 446-460.

[2] B. Pawelec, R. M. Navarro, J. M. Campos-Martin, J. L. G. Fierro, *Catal. Sci. Tech.*, 2011, **1**, 23-42.

[3] I. V. Babich, J. A. Moulijn, *Fuel*, 2003, **82**, 607-631.

[4] A. J. Hernandez-Maldonado, F. H. Yang, G. S. Qi, R. T. Yang, *Appl. Catal. B*, 2005, **56**, 111-126.

[5] S. Mondal, Y. Hangun-Balkir, L. Alenxandrova, D. Link, B. Howard, P. Zandhuis, A. Cugini, C. P. Horwitz, T. J. Collins, *Catal. Today*, 2006, **116**, 554-561.

[6] H. Y. Lu, J. B. Gao, Z. X. Jiang, F. Jing, Y. X. Yang, G. Wang, C. Li, *J. Catal.*, 2006, **239**, 369-375.

[7] F. Zannikos, E. Lois, S. Stournas, *Fuel Process Technol.*, 1995, **42**, 35-45.

[8] S. Otsuki, T. Nonaka, N. Takashima, W. H. Qian, A. Ishihara, T. Imai, T. Kabe, *Energy Fuels* 2000, **14**, 1232-1239.

[9] D. Huang, G. S. Luo, Y. J. Wang, *Microporous Mesoporous Mater.*, 2005, **84**, 27-33.

[10] D. Huang, Y. J. Wang, L. M. Yang, G. S. Luo, *Ind. Eng. Chem. Res.*, 2006, **45**, 1880-1885.

[11] D. Huang, Y. J. Wang, L. M. Yang, G. S. Luo, *Microporous Mesoporous Mater.*, 2006, **96**, 301-306.

[12] D. Huang, Z. Zhai, Y. C. Lu, L. M. Yang, G. S. Luo, *Ind. Eng. Chem. Res.*, 2007, **46**, 1447-1451.

[13] D. Huang, Y. C. Lu, Y. J. Wang, G. S. Luo, *Ind. Eng. Chem. Res.*, 2007, **46**, 6221-6227.

[14] D. Huang, Y. C. Lu, Y. J. Wang, L. M. Yang, G. S. Luo, *Ind. Eng. Chem. Res.*, 2008, **47**, 3870-3875.

[15] D. Huang, Y. J. Wang, Y. C. Cui, G. S. Luo, *Microporous Mesoporous Mater.*, 2008, **116**, 378-385.

[16] J. M. Campos-Martin, M. C. Capel-Sanchez, P. Perez-Presas, J. L. G. Fierro, *J. Chem. Technol. Biotechnol.*, 2010, **85**, 879-890.

[17] Z. Ismagilov, S. Yashnik, M. Kerzhentsev, V. Parmon, A. Bourane, F. M. Al-Shahrani, A. A. Hajji, O. R. Koseoglu, *Catal. Rev-Sci. Eng.*, 2011, **53**, 199-255.

[18] F. Lin, D. G. Wang, Z. X. Jiang, Y. Ma, J. Li, R. G. Li, C. Li, *Energy Environ. Sci.*, 2012, **5**, 6400-6406.

[19] X. J. Wang, F. T. Li, J. X. Liu, C. G. Kou, Y. Zhao, Y. J. Hao, D. S. Zhao, *Energy Fuels*, 2012, **26**, 6777-6782.

[20] X. M. Gao, F. Fu, L. P. Zhang, W. H. Li, *Phys. Rev. B: Condens. Matter.*, 2013, **419**, 80-85.

[21] D. J. Wang, L. L. Yue, L. Guo, F. Fu, G. L. Xue, *J. Inorg. Mater.*, 2013, **28**, 1079-1086.

[22] M. T. Timko, E. Schmois, P. Patwardhan, Y. Kida, C. A. Class, W. H. Green, R. K. Nelson, C. M. Reddy, *Energy Fuels*, 2014, **28**, 2977-2983.

[23] R. T. Yang, A. J. Hernandez-Maldonado, F. H. Yang, *Science*, 2003, **301**, 79-81.

[24] N. A. Khan, Z. Hasan, S. H. Jhung, *Chem. Eur. J.*, 2014, **20**, 376-380.

[25] K. S. Triantafyllidis, E. A. Deliyanni, *Chem. Eng. J.*, 2014, **236**, 406-414.

[26] M. Y. Sun, G. H. Cheng, R. J. Lu, T. M. Tang, S. A. Baig, X. H. Xu, *Fuel Process Technol.*, 2014, **118**, 28-33.

[27] J. M. Campos-Martin, M. C. Capel-Sanchez, J. L. G. Fierro, *Green Chem.*, 2004, **6**, 557-562.

[28] J. B. Gao, Y. N. Zhang, G. Q. Jia, Z. X. Jiang, S. G. Wang, H. Y. Lu, B. Song, C. Li, *Chem. Commun.*, 2008, 332-334.

[29] X. Jia, H. M. Li, W. S. Zhu, L. N. He, H. M. Shu, J. D. Lu, *Fuel*, 2009, **88**, 431-436.

[30] Y. N Zhang, H. Y. Lu, L. Wang, Y. L. Zhang, P. Liu, H. X. Han, Z. X. Jiang, C. Li, *J. Mol. Catal. A: Chem.*, 2010, **332**, 59–64.

[31] T. O. Sachdeva, K. K. Pant, *Fuel Process Technol.*, 2010, **91**, 1133–1138.

[32] X. L. Xue, W. Zhao, B. C. Ma, Y. Ding, *Catal. Commun.*, 2012, **29**, 73–76.

[33] J. X. Yang, D. D. Hu, S. F. Song, L. J. Sun, *Colloid Polym. Sci.*, 2013, **291**, 2861–2869.

[34] H. W. Zheng, Z. Sun, X. L. Chen, Q. Zhao, X.H. Wang, Z. J. Jiang, *Appl. Catal. A*, 2013, **467**, 26–32.

[35] J. Z. Zhuang, B. Hu, J. J. Tan, X. Y. Jin, *Transition Met. Chem.*, 2014, **39**, 213–220.

[36] F. L. Yu, R. Wang, *Chem. Lett.*, 2014, **43**, 834-836.

[37] R. Vargas, O. Nunez, *J. Mol. Catal. A: Chem.*, 2008, **294**, 74-81.

[38] J. Zhang, D. S. Zhao, J. L. Wang, L. Y. Yang, *J. Mater. Sci.*, 2009, **44**, 3112-3117.

[39] C Wang, Y. H. Ao, P. F. Wang, J. Hou, J. Qian, *Colloids Surf. A Physicochem. Eng. Aspects*, 2010, **360**, 184-189.

[40] T. H. T. Vu, T. T. T. Nguyen, P. H. T. Nguyen, M. H. Do, H. T. Au, T. B. Nguyen, D. L. Nguyen, J. S. Park, *Mater. Res. Bull.*, 2012, **47**, 308-314.

[41] L. Wang, H. J. Cai, S. Z. Li, N. Mominou, *Fuel*, 2013, **105**, 752-756.

[42] C. Y. Su, X. Ran, J. L. Hu, C. L. Shao, *Environ. Sci. Technol.*, 2013, **47**, 11562-11568.

[43] U. Arellano, J.A. Wang, M.T. Timko, L.F. Chen, S.P. Paredes Carrera, M. Asomoza, O.A. Gonz âez Vargas, M.E. Llanos, *Fuel*, 2014, **126**, 16-25.

[44] C. Wang, W. Zhu, Y. Xu, H. Xu, M. Zhang, Y. Chao, S. Yin, H. Li, J. Wang, *Ceram. Int.*, 2014, **40**, 11627-11635.

[45] E. Loren ço n, D. C. B, Alves, K. Krambrock, E. S. Ávila, R. R. Resende, A. S. Ferlauto, R. M. Lago, *Fuel*, 2014, **132**, 53-61.

[46] C. Ma, B. Dai, P. Liu, N. Zhou, A. Shi, L. Ban, H. Chen, *J. Ind. Eng. Chem.*, 2014, **20**, 2769-2774.

[47] M. Zarrabi, M. H. Entezari, E. K. Goharshadi, *RSC Adv.*, 2015, **5**, 34652-34662.

[48] S. H. Xun, W. S. Zhu, D. Zheng, H. P. Li, W. Jiang, M. Zhang, Y. J. Qin, Z. Zhao, H. M. Li, *RSC Adv.*, 2015, **5**, 43528-43536.

[49] H. F. M. Zaid, F. K. Chong, M. I. A. Mutalib, *Fuel*, 2015, **156**, 54-62.

[50] M. Zarrabi, M. H. Entezari, *J. Colloid Interf. Sci.*, 2015, **457**, 353-359.

[51] W. S. Zhu, Y. H. Xu, H. M. Li, B. L. Dai, H. Xu, C. Wang, Y. H. Chao, H. Liu, *Korean J. Chem. Eng.*, 2014, **31**, 211-217.

[52] J. H. Guo, S. Watanabe, M. J. Janik, X. L. Ma, C. S. Song, *Catal. Today*, 2010, **149**, 218-223.

[53] S. Watanabe, X. L. Ma, C. S. Song, *J. Phys. Chem. C*, 2009, **113**, 14249-14257.

[54] L. Benz, A. Park, J. R. Corey, M. P. Mezher, V. C. Park, *Langmuir*, 2012, **28**, 10209-10216.

[55] X. M. Yan, P. Mei, L. Xiong, L. Gao, Q. F. Yang, L. J. Gong, *Catal. Sci. Technol.*, 2013, **3**, 1985-1992.

[56] S. Nair, A. H. M. Shahadat Hussain, B. J. Tatarchuk, *Fuels*, 2013, **105**, 695-704.

[57] A. H. M. Shahadat Hussain, B. J. Tatarchuk, *Fuels*, 2013, **107**, 465-473.

[58] J. Xiao, X. X. Wang, M. Fujii, Q. J. Yang, C. S. Song, *AIChE J.*, 2013, **59**, 1441-1445.

[59] W. R. Webster, A. Park, M. B. Stratton, V. C. Park, A. M. Mosier, R. S. Shine, L. Benz, *Energy Fuels*, 2013, **27**, 6575-6580.

[60] J. Xiao, X. X. Wang, Y. S. Chen, M. Fujii, C. S. Song, *Ind. Eng. Chem. Res.*, 2013, **52**, 15746-15755.

[61] Y. W. Sun, Y. J. Wang, Y. C. Lu, T. Wang, G. S. Luo, *J. Am. Ceram. Soc.*, 2008, **91**, 103-109.

[62] C. Shen, Y. J. Wang, J. H. Xu, Y. C. Lu, G. S. Luo, *Particuology*, 2012, **10**, 317-326.

[63] C. Shen, Y. J. Wang, J. H. Xu, Y. C. Lu, G. S. Luo, *Green Chem.*, 2012, **14**, 1009-1015.

[64] F. Geobaldo, S. Bordiga, A. Zecchina, E. Giamello, G. Leofanti, G. Petrini, *Catal. Lett.*, 1992, **16**, 109-115.

[65] G. Deo, A. M Turek, I. E. Wachs, D. R. C. Huybrechts, P. A. Jacobs, *Zeolites*, 1993, **13**, 365-373.

[66] M. C. Capel-Sanchez, J. M. Campos-Martin, J. L. G. Fierro, M. P. de Frutos, A. Padilla Polo, *Chem. Commun.*, 2000, **10**, 855-856.

[67] L. Cedeno-Caero, M. Ramos-Luna, M. Mendez-Cruz, J. Ramirez-Solis, *Catal. Today*, 2011, **172**, 189–194

[68] T. Sauer, G. C. Neto, H. J. Jose, R. Moreira, *J. Photochem. Photobiol. A Chem.*, 2002, **149**, 147-154.

[69] S. Dhir, R. Uppaluri, M. K. Purkait, *J. Hazard. Mater.*, 2009, **161**, 1360-1368.

[70] S. A. Al-Bogami, J. Moreira, H. I. Lasa, *Ind. Eng. Chem. Res.*, 2013, **52**, 17760-17772.

Table legends

Table 1: Surface areas of catalysts with different Ti content.

Table 2: Comparisons in catalytic performance with other works (selectivity is 100% in all the works).

Table 3: Apparent pseudo-first-order values obtained at different temperatures.

Table 4: Langmuir-Hinshelwood parameters obtained at different temperatures.

Figure legends

Fig. 1: Conceptual model of ODS using the as-prepared amphiphilic catalyst.

Fig. 2: Surface morphologies and pore size distribution of porous glass beads supported with TiO_2 nanoparticles.

Fig. 3: XRD pattern of the supported TiO_2 nanoparticles.

Fig.4: TEM images of TiO_2 nanoparticles supported on porous glass beads; (a): lattice fringes with a width of 0.34 nm; (b), (c) and (d): Ti content of 1.27 wt.%, 3.67 wt.% and 9.85 wt.%, respectively; (e), (f) and (g): Histograms of particle size distribution for Ti content of 1.27 wt.% 3.67 wt.% and 9.85 wt.%, respectively.

Fig.5: Effects of reaction duration and catalyst amount; reaction temperature: 333 k; 1.0 g catalyst; molar ratio of H_2O_2-to-DBT: 10; initial concentration of DBT: 150 ppm.

Fig.6: (a) catalytic performance of TiO_2 immobilized on porous glass through suspension method (I), TiO_2 immobilized on HCl-treated porous glass through suspension method (II) and TiO_2 powder (III), respectively; (b) catalytic performance of hydrophobicated catalyst with different contact angles: 0 °(I), 106 °(II) and 154 °(III), respectively. Reaction temperature: 333 k; molar ratio of H_2O_2-to-DBT: 10; initial concentration of DBT: 50 ppm.

Fig.7: Effect of initial concentration; reaction temperature: 333 k; 1.0 g catalyst; Ti content: 4.35 wt.%; molar ratio of H_2O_2-to-DBT: 10.

Fig. 8: (a) Effect of oxidant amount; reaction temperature: 333 k; 1.0 g catalyst; Ti content: 5.99 wt.%; initial concentration of DBT: 150 ppm; (b) and (c) distribution of porous glass supported with TiO_2 nanoparticles in the model oil.

Fig. 9: (a): Effect of reaction temperature; 0.6 g catalyst; Ti content: 5.99 wt.%; initial concentration of DBT: 150 ppm; molar ratio of H_2O_2-to-DBT: 10; (b): Arrhenius plot.

Fig. 10: Oxidation of 4,6-DMDBT; 1.0 g catalyst; Ti content: 6.45 wt.%; initial concentration of 4,6-DMDBT: 150 ppm; molar ratio of H_2O_2-to-4,6-DMDBT: 10.

Fig. 11: Regeneration performance of TiO_2 supported on porous glass; reaction temperature: 333 k; 1 g catalyst; molar ratio of H_2O_2-to-DBT: 10; initial concentration of DBT: 150 ppm; Ti content: 6.45 wt.%; reaction duration: 2 min.

List of tables

Table 1

Ti content (wt. %)	Surface area (m^2/g)
1.27	131.5
3.67	124.9
6.45	116.9
8.24	107.6
9.85	101.2

Table 2

Reaction duration (min)	UV irradiation	Catalyst amount (g)	Mean particle size of TiO_2 (nm)	Support	X (%)	STY (g_{DBTS}/(g_{TS-1} min))	Reference
2	No	0.065	3.0	Porous glass	100	4.74×10^{-2}	This work
300	Yes	0.100	5.83	No support	90	8.80×10^{-4}	[19]
60	Yes	0.100	Not mentioned	No support	70	1.37×10^{-4}	[37]
150	Yes	0.008	Not mentioned	Bamboo	70	5.11×10^{-3}	[38]
480	Yes	0.952	130	Multi-walled carbon nanotubes	80	1.03×10^{-4}	[40]

Table 3

Temperature (K)	App. k_{obs} (h^{-1})	R^2
303	16.5	0.9981
313	24.5	0.9959
323	40.9	0.9935
333	61.2	0.9943

Table 4

Temperature (K)	$K \times 10^3$ (L/mg)	k_r (mg/L/s)
303	6.80	0.67
313	4.54	1.50
323	3.88	2.93
333	2.91	5.85

List of figures

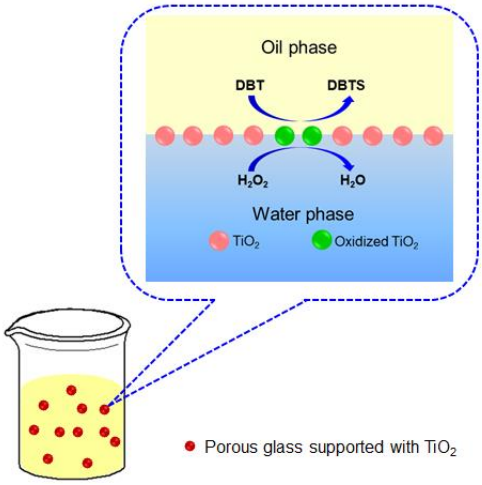

Fig. 1

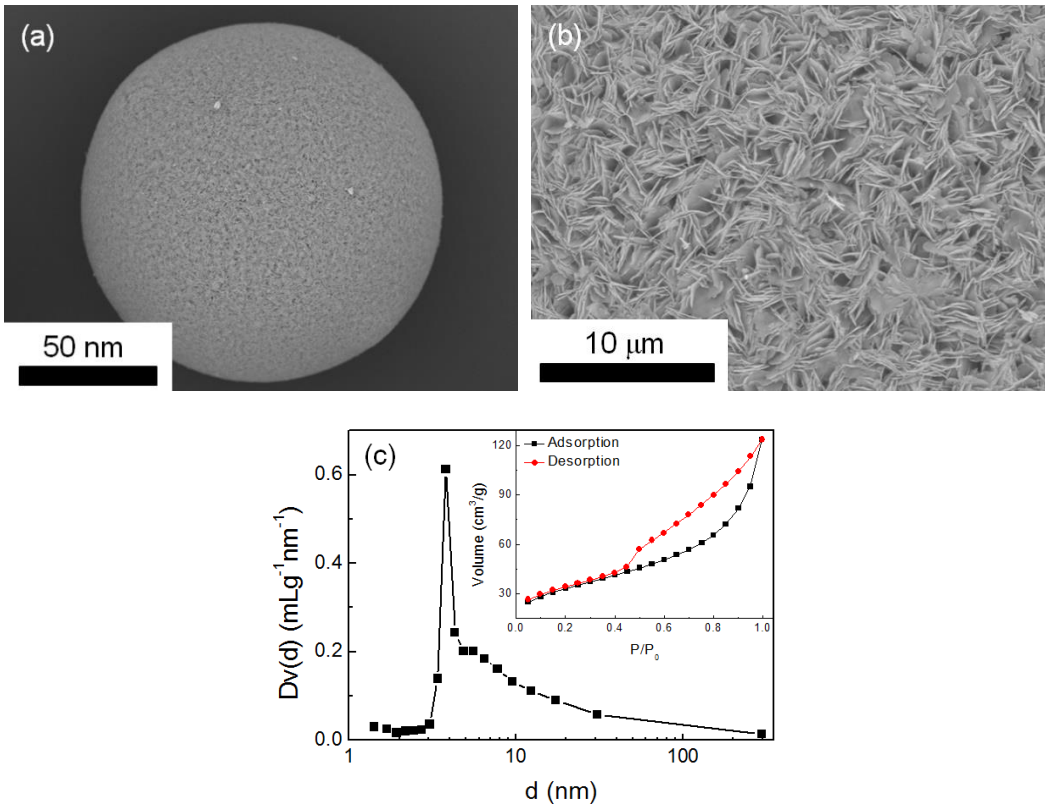

Fig. 2

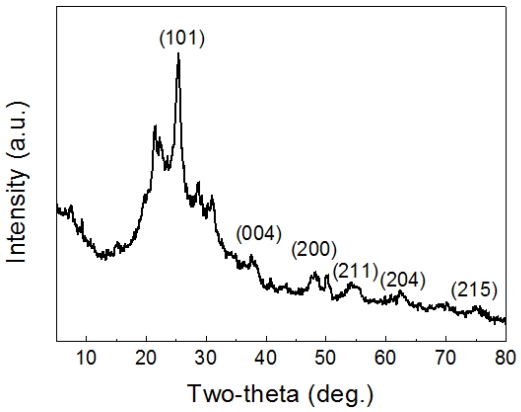

Fig. 3

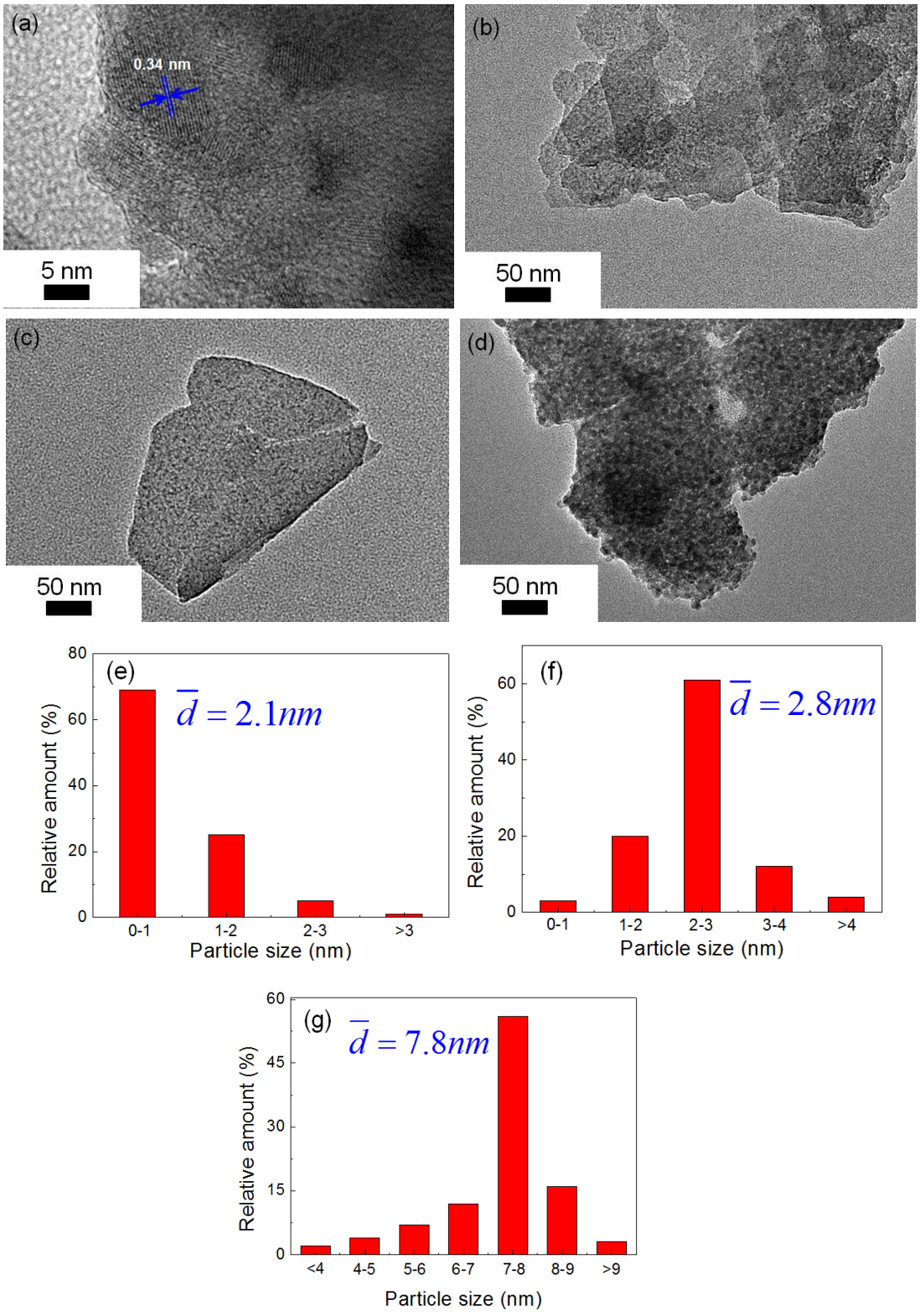

Fig. 4

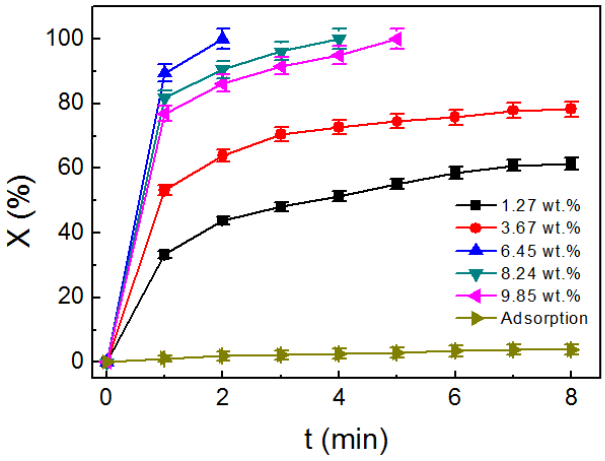

Fig. 5

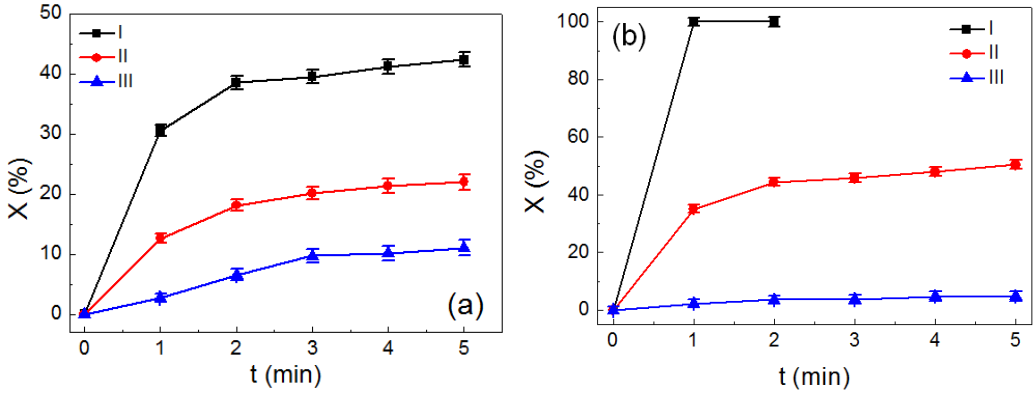

Fig. 6

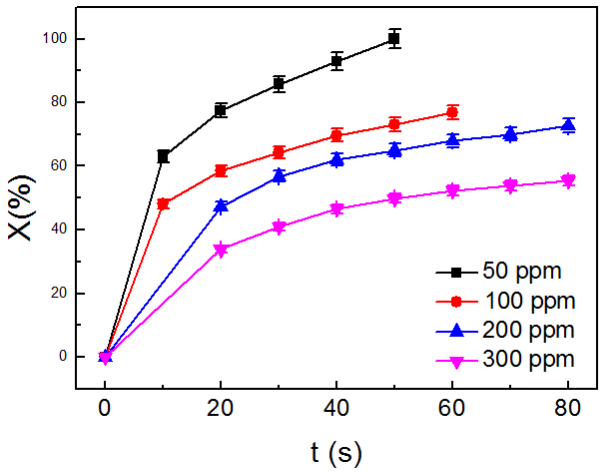

Fig.7

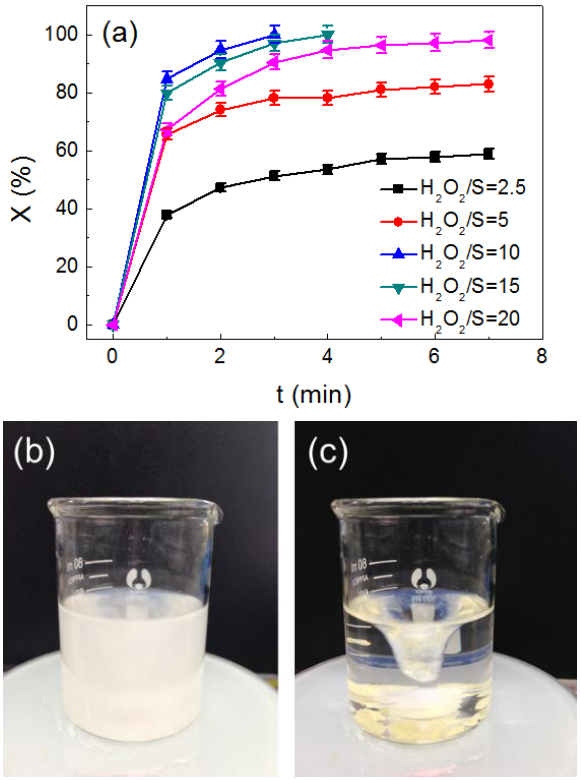

Fig. 8

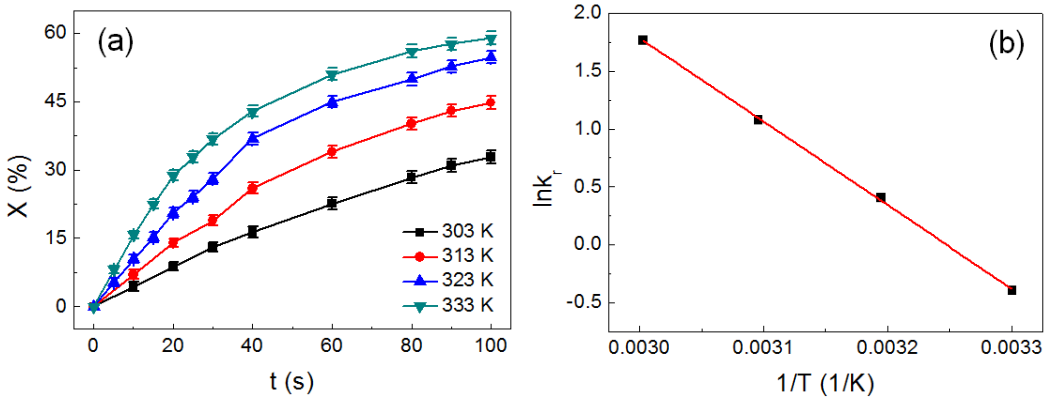

Fig. 9

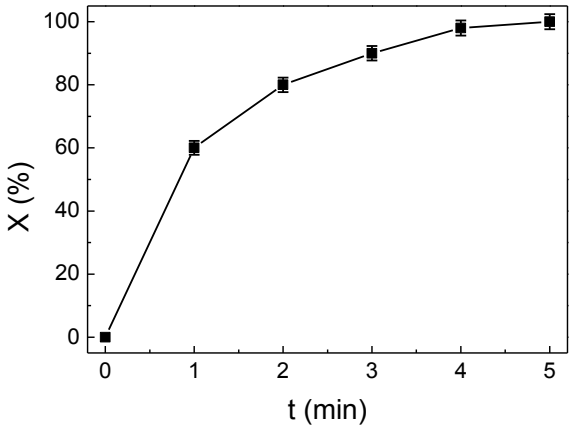

Fig. 10

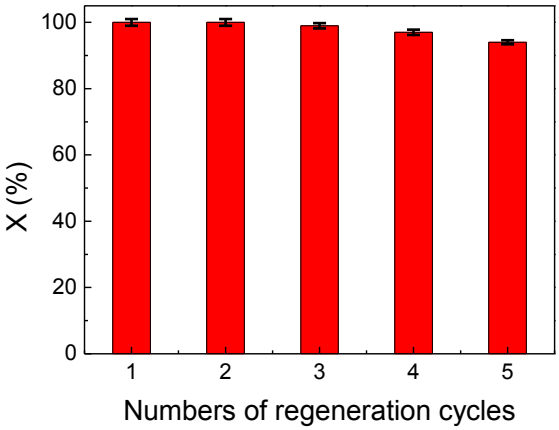

Fig. 11

Graphical abstract

Porous glass supported with TiO_2 nanoparticles acted as an amphiphilic catalyst. Because of good adsorptive properties for both reactants, the support gathers the two reactants on the active sites.